Transformation Optics and Subwavelength Control of Light

J. B. Pendry *et al.*

Science **337**, 549 (2012);
DOI: 10.1126/science.1220600

Transformation Optics and Subwavelength Control of Light

J. B. Pendry,[1]* A. Aubry,[2] D. R. Smith,[3] S. A. Maier[1]

Our intuitive understanding of light has its foundation in the ray approximation and is intimately connected with our vision. As far as our eyes are concerned, light behaves like a stream of particles. We look inside the wavelength and study the properties of plasmonic structures with dimensions of just a few nanometers, where at a tenth or even a hundredth of the wavelength of visible light the ray picture fails. We review the concept of transformation optics that manipulates electric and magnetic field lines, rather than rays; can provide an equally intuitive understanding of subwavelength phenomena; and at the same time can be an exact description at the level of Maxwell's equations.

The field of optics is not just confined to imaging but extends to communication, sensing, cancer treatment, and even welding of automobile parts. Manipulation of light is vital to exploitation of its potential, but light is difficult to control on length scales less than the wavelength, where diffraction causes conventional optical components to fail. This is the length scale of atoms and molecules, living cells, electrons, computer microchips, and micromechanical devices. Subwavelength control demands new optical materials, and efforts have turned to metals such as gold and silver, where the plasmon collective excitations of the conduction electrons couple to light and can compress the captured energy into just a few cubic nanometers. We review the latest developments in transformation optics applied to plasmonic systems whereby Snell's law, the traditional design tool of optics, is being replaced by transformation optics, a new tool that is fully compatible with the wave nature of light as described by Maxwell's equations.

Snell's law tells how light is refracted by transparent media. It gives a picture of light's progress in terms of rays, which can be thought of as streams of photons. This simple, intuitive picture is a vital component of the design process and explains why the law is still widely used despite its neglect of reflection at interfaces and diffraction by small features. Only Maxwell's equations give a precise description of all the classical features of light, but they lack the visual intuition provided by the ray picture. Transformation optics aims to give a picture equally intuitive to that of ray optics by using instead the raw elements of Maxwell's equations—the electric and magnetic field lines introduced by Faraday—and gives rules for how these lines can be manipulated almost at will by a suitable choice of material.

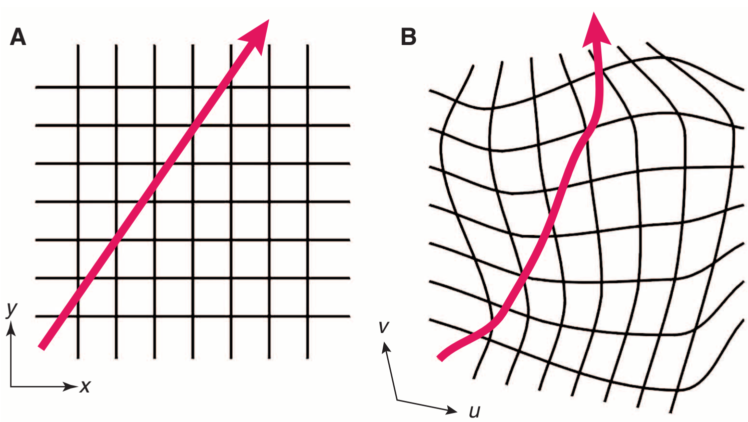

Fig. 1. (**A**) Field lines of a uniform electric displacement field. (**B**) Distortion of space as if it were a rubber sheet bends the field line, and the coordinate system records the distortion.

To understand how transformation optics works, imagine a uniform electric displacement field in free space. The location of the field lines is recorded on a system of coordinates (Fig. 1). If we postulate that the field lines are fixed to the coordinates so that the coordinate system carries the field lines with it under a distortion, then we can shape the trajectories of the field simply by distorting the coordinates. It has long been known that writing Maxwell's equations in a new coordinate system does not change the form but changes only the values of permittivity and permeability as follows

$$\varepsilon'^{i'j'} = [\det(\Lambda)]^{-1}\Lambda_i^{i'}\Lambda_j^{j'}\varepsilon^{ij}$$
$$\mu'^{i'j'} = [\det(\Lambda)]^{-1}\Lambda_i^{i'}\Lambda_j^{j'}\mu^{ij}$$

where ε and μ are the permittivity and the permeability, respectively, in the original coordinate frame and ε′ and μ′ are the corresponding quantities in the transformed frame (*1*, *2*). Λ is given by the first derivatives of the coordinate transformation

$$\Lambda_j^{j'} = \frac{\partial x^{j'}}{\partial x^j}$$

The transformed values of ε′ and μ′ ensure that Maxwell's equations are obeyed by the new configuration of the field lines.

Transformation optics comes about from the realization that the field lines are glued to the coordinate system; this insight gives rise to the intuitive picture that we seek as a replacement for Snell's law. Any conserved electromagnetic field that can be represented by a field line has the property of adhesion to the coordinate frame. Thus, the Poynting vector also transforms in this fashion. The field lines of the Poynting vector can, in fact, be thought of as a more precise definition of rays of light.

Early applications of transformation optics involved adapting computer codes from Cartesian to cylindrical geometries (*3*). However, with the advent of metamaterials, the realization emerged that transformation optics could be more than simply a computational tool and was subsequently applied as a means of determining the material properties needed to reshape the perfect lens (*4*), allowing it to magnify objects (*5*). Detailed reviews can be found in (*6*, *7*).

We note that transformation optics can be applied to other equations of physics, such as the Helmholtz equation, an approximation to Maxwell's equations (*8*) and to acoustics (*9*).

Transformation optics can render trivial the design of optical structures that would be otherwise difficult or seemingly impossible (*10*, *11*). For example, transformation optics was used to design a cloak of invisibility, whose material properties flowed naturally from a relatively simple transformation (*8*, *12*). The technique is ideally suited to the task of steering field lines away from a hidden region while leaving them undisturbed in the vicinity of the observer. We exploit the general applicability of the technique to treat subwavelength fields occurring in plasmonic nanosystems, giving us a precise design tool. Although the transformation of near-fields is an extremely versatile tool

[1]The Blackett Laboratory, Department of Physics, Imperial College London, London SW7 2AZ, UK. [2]Institut Langevin, École Supérieure de Physique et de Chimie Industrielles de la Ville de Paris, ParisTech, CNRS UMR 7587, 1 rue Jussieu, 75005 Paris, France. [3]Center for Metamaterials and Integrated Plasmonics and Department of Electrical and Computer Engineering, Duke University, Box 90291, Durham, NC 27708, USA.

*To whom correspondence should be addressed. E-mail: j.pendry@imperial.ac.uk

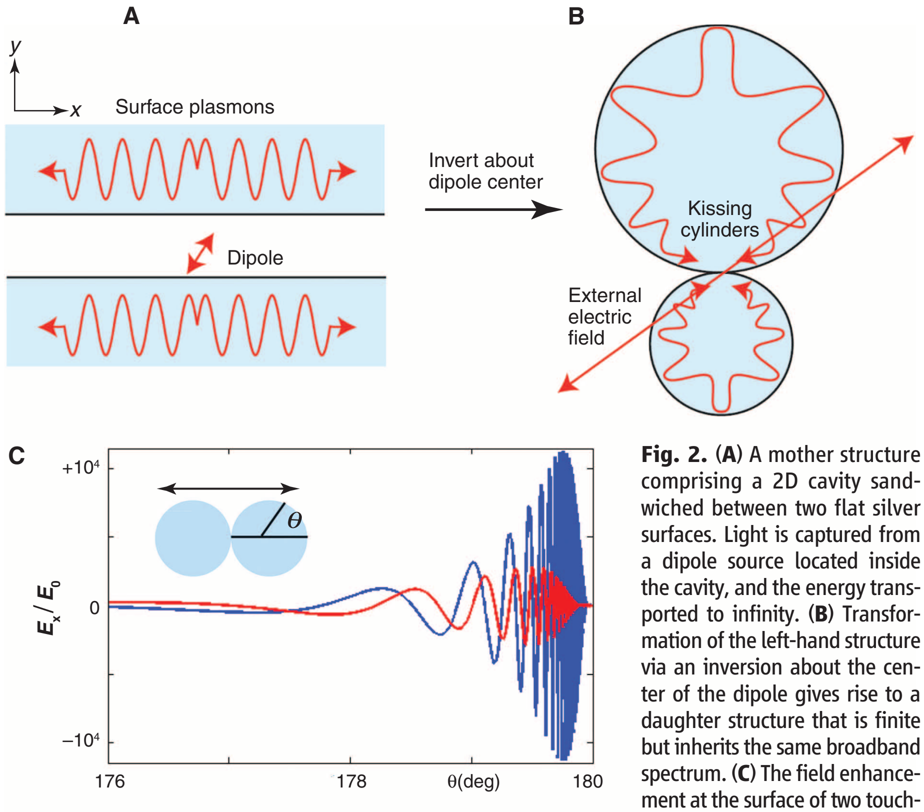

Fig. 2. (**A**) A mother structure comprising a 2D cavity sandwiched between two flat silver surfaces. Light is captured from a dipole source located inside the cavity, and the energy transported to infinity. (**B**) Transformation of the left-hand structure via an inversion about the center of the dipole gives rise to a daughter structure that is finite but inherits the same broadband spectrum. (**C**) The field enhancement at the surface of two touching silver cylinders of equal radii at a frequency $0.7\omega_{sp}$, where ω_{sp} is the surface plasmon frequency of an isolated cylinder. The blue curve is calculated by using the experimentally measured permittivity; the red curve shows the effect of doubling the imaginary part of the permittivity. The incident electric field orientation E_x is shown by the black arrows.

applicable for the study of numerous phenomena, we focus on the light-harvesting properties of nanoparticles to illustrate the techniques.

Harvesting Light

If a photon is to have a strong interaction with a molecule, its energy must somehow be concentrated into the same dimensions as those of the molecule. This harvesting process is well known in nature, for example, in the chlorophyll complex through which light is collected and delivered to the reaction center to create sugars from carbon dioxide. We show how to mimic nature by exploiting surface plasmons. Ideally, the structure should harvest a broad spectrum of radiation.

Raman spectroscopy of rough silver surfaces first revealed the potential for enhanced photon-molecule interaction (*13*). Raman signals can be spectacularly enhanced, sometimes by a factor on the order of a million, when the interaction takes place at a rough metal surface. It is now believed that the enhancement is due to the concentration of the electric field at singularities in the geometry of the surface. Many computer simulations of Maxwell's equations have confirmed this picture (*14*–*21*). Early work showed the importance of geometrical singularities in producing enhancement (*22*–*24*). Physical insight has been provided by the hybridization model (*25*). A review of light concentration is given in (*26*).

We start from a simple configuration that has the required broadband harvesting properties, at first paying little attention to the geometry because we know that the geometry can be changed by a transformation, leaving the spectrum unaltered (*27*–*30*). Figure 2A shows a waveguide comprising a planar cavity between two silver surfaces. The system is infinite in directions parallel to the surfaces, and therefore the spectrum is continuous and is formed by the hybridization of surface plasmons on opposing surfaces. The lower band extends from zero up to the surface plasmon frequency, and the upper band, from the surface plasmon frequency to the bulk plasmon frequency, ω_p. We shall mainly be concerned with the lower band, which is usually much broader than the upper band and therefore more flexible in its applications.

A dipole source, such as an excited atom, placed in the waveguide now excites surface plasmon modes, which transport energy away to infinity. Although this is harvesting of a sort, it is not particularly useful. To remedy this, we make a radical transformation of the geometry.

First, we assume that the electric fields dominate so that we neglect retardation and that the fields are oriented in the *xy* plane and are invariant along the out-of-plane dimension. Because the field pattern is effectively two-dimensional (2D), we are able to apply the theory of optical conformal transformations to the geometry (*5*, *8*). The conformal transformation ensures that all material properties are maintained as isotropic. Consider the conformal transformation defined by

$$z' = 1/z$$

where $z = x + iy$ and the origin is taken to be at the center of the dipole. This transformation takes planes into cylinders, points at infinity to the new origin, and points at the origin to the new infinity. A dipole can be represented as two very large opposite charges very close together. Under this transformation, the new dipole consists of two very large charges at infinity, which create a uniform electric field at the origin. In other words, in the new coordinate system (Fig. 2), the two semi-infinite planes become two kissing cylinders, and excitations are created by a uniform electric field such as might be imposed by an incident plane wave. Our assumption that the electric field dominates is valid provided that the cylinder radii are much less than the wavelength of light. Another transformation optics–based approach is found in (*31*).

Conformal transformations in 2D have the property that in-plane components of the permittivity tensor are unchanged in the new coordinate system. This is not true of conformal transformations in 3D, although transformation optics has nevertheless been successfully applied to 3D systems (*32*).

The original system is excited by a dipole and harvests its energy to infinity, but the transformed system is excited by the uniform electric field of a plane wave and the energy harvested is focused to the origin. Just as energy never reaches infinity in the original, so it never reaches the origin in the new system. As the excited waves travel with slower and slower group velocity, their energy density increases, giving rise to a huge field enhancement (Fig. 2C). Note also the compression of the surface plasmon wavelength. In an ideal loss-free system, energy density would rise remorselessly to infinity (the waves are never reflected), but in practice losses intervene and eventually terminate the increase in energy density for realistic values of the silver permittivity. Despite the presence of loss, very large enhancements are seen: A field enhancement of 10^4 would enhance the sensitivity to Raman signals by a factor of 10^{16}. As we shall see, loss is not the ultimately limiting factor. Nevertheless, in practice, very substantial enhancements can be expected for singular structures.

Physical Insight and Hidden Symmetry

It has long been known that singular structures greatly enhance the energy density of radiation, and indeed sophisticated computer simulations reveal many of the details (*14*–*21*). So what does transformation optics add to the story?

Take the kissing cylinder configuration shown in Fig. 2: Computer simulations variously work either by quantizing the fields on a mesh or by making an expansion in many cylindrical harmonics. The picture that emerges is a complex representation of the fields. Transformation optics reveals that this complexity is not intrinsic to the spectrum but is imposed by the transformation from a simple system to a more complex one. The kissing cylinders have little intrinsic symmetry: just an axis of rotation and a couple of mirror planes. However, the original planar waveguide has translational symmetry that enables us to classify all eigenstates by a Bloch wave vector, k. Although this symmetry is hidden by the transformation, it continues as a good quantum number for the eigenstates of the new system, offering valuable insight into their nature (*27*).

In computational studies, each new structure requires computation to begin again. In transformation optics, our "mother" structure is related to an infinity of "daughter" structures, giving us the ability to classify a whole category of structures as belonging to the same family. In general, mother structures that are infinite, as is the case in Fig. 2, give rise to continuous spectra. Transformations to finite structures give rise to singularities because infinity is mapped into something that is finite. In Fig. 3, left, we show a series of singular structures obtained by transforming planar waveguides, and therefore all of them have continuous spectra and show large field enhancements in the vicinity of the singularities.

On the other hand, starting from a finite planar structure means that the spectrum is discrete, as is the case for all nonsingular finite structures. The transformed structures of Fig. 3, right, derive from planar mother structures that are finite; in consequence they inherit the discrete spectra, and their geometry is free of the singularities that would be essential were the spectra to be continuous.

The various transformations used to generate these structures can be seen in (*33*–*35*).

Radiative Corrections

So far we have assumed a very small system and neglected radiative corrections. However, radiative scattering increasingly competes with the harvesting process as system size increases and ultimately limits how large a system can be and still have useful harvesting capability.

Radiation is a loss mechanism and can be approximated by introducing an absorbing medium outside a large cylinder that encases the whole system (Fig. 4B) (*36*). If only dipole radiation is appreciable, then this approximation is exact. Applying transform optics in reverse takes the large hollow cylinder into a small cylinder containing the absorbing material (Fig. 4A). As it happens for all systems for which harvesting is substantial, dipole radiation dominates and this is a very accurate approximation. Figure 4C shows the reduction in enhancement resulting from radiative corrections calculated by using the dipole absorber approximation and by direct computer simulation. Radiative corrections degrade this harvester's performance. For systems of 200-nm dimensions and larger, most of the incident radiation is scattered rather than harvested.

Nonlocal Corrections

We have seen how radiative corrections spoil the harvesting process for large systems. However, there is a limit to how small we can make our system and still have it function efficiently. Quite apart from difficulties of constructing nanoscale systems, nonlocal effects become substantial for systems smaller than a few nanometers in diameter (*37*–*39*).

Nonlocality arises because of quantum effects in the metal's conduction electrons. If we apply an electric field to a metal surface, electrons migrate to the surface and screen the interior of the metal from the field. Because the electrons are not infinitely compressible, the screening electrons are not located precisely at the surface but are distributed in a layer whose thickness is of the order of the Fermi Thomas screening length, or about 0.1 nm in a typical metal.

The local approximation amounts to assuming that the screening electrons are confined to an infinitely thin surface layer. This is a good approximation unless the system dimensions are very small indeed; unfortunately, that is the case for harvesting systems where the enhanced fields are found for surfaces that approach very closely. As a result, nonlocal effects ultimately limit the enhancement. Technically, the charge distribution inside a metal is represented by the longitudinal modes: the bulk plasmons. For most purposes in optics, bulk plasmons play no role: Their frequency is assumed independent of wave vector, q, and they cannot be excited by external radiation. But for small systems, their dispersion, $\omega_p(q)$, becomes appreciable and has to be taken into account. If $\omega > \omega_p(q = 0)$, bulk plasmons have finite group velocity and carry energy away from the surface into the bulk. If $\omega < \omega_p(q = 0)$, bulk plasmon modes decay as $\exp(-\delta z)$, the exponent δ defining a decay length representing the finite size of the nonlocal surface charge. In contrast, the transverse modes for $\omega < \omega_p(q = 0)$ represent

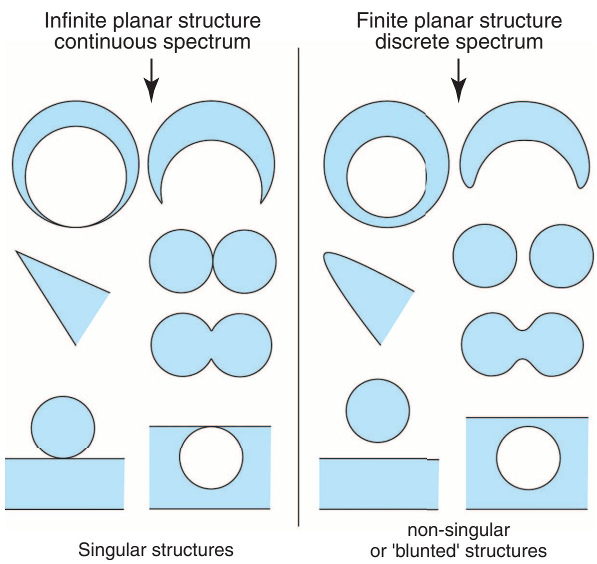

Fig. 3. A single mother structure, such as the planar waveguide shown in Fig. 2, can be transformed into an infinite variety of daughter structures; that is, they all have identical spectra. If the mother planar structure is infinite, the spectrum is continuous and the daughter structures are singular, that is, possessed of sharp features; if finite, the spectrum is discrete and the daughter structures nonsingular, that is, no sharp features.

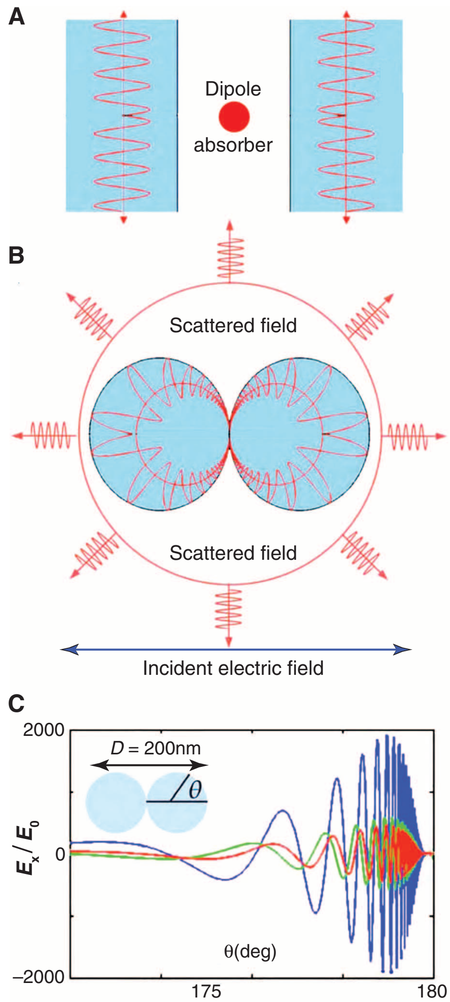

Fig. 4. (**A**) A small lossy dielectric sphere transforms into (**B**) a large hollow dielectric absorber. In this way, radiation losses can be taken into account. (**C**) Field enhancement as a function of angle around the cylinder. Blue line, no radiative correction; red line, dipole absorber correction; and green line, computer simulation including retardation.

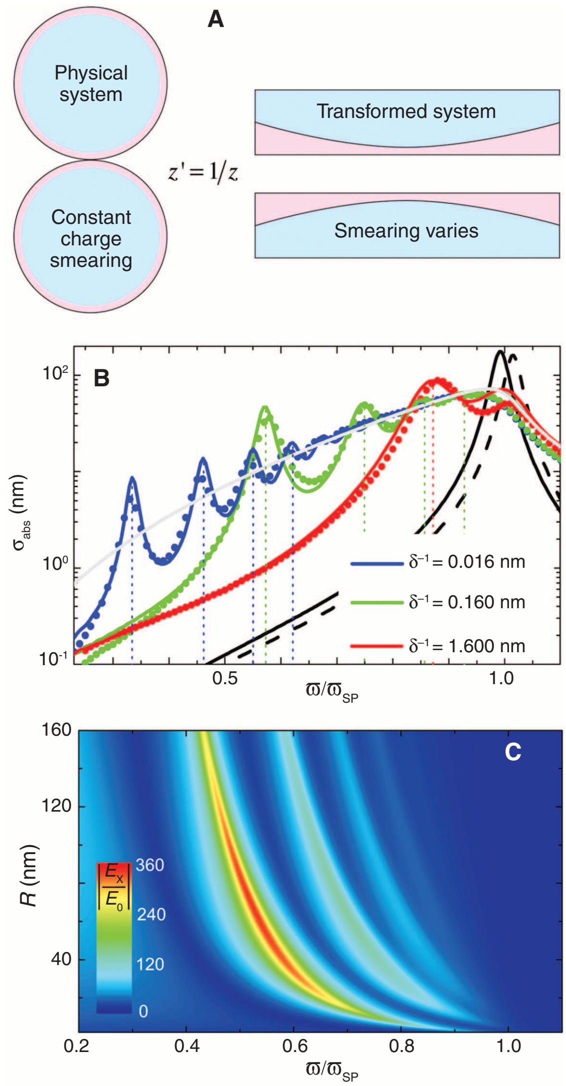

Fig. 5. (**A**) (Left) Nonlocality smears the screening charge so that in effect the surfaces no longer touch, and therefore field enhancement is reduced. (Right) Transformation optics distorts the length scales in the transformed system, and as a result the smearing of the surface charge varies with position. (**B**) The absorption cross section for cylindrical dimers of radius 10 nm for various values of the nonlocal decay length, δ^{-1}. Full lines show the transformation optics result; dots are computed by using comsol. The gray line shows the local result for the dimers; the black line, the local results for a single cylinder; and the dashed line, the nonlocal results for a single cylinder. (**C**) Absolute value of the field enhancement at the touching point for cylinders of various radii (*R*).

the decay of the fields into the bulk. Ultimately for very small particles, the dielectric description breaks down entirely as the electron levels are quantized, and electron tunneling between components of the system comes to dominate. The debate is ongoing as to how small a system must be for a dielectric description to fail, but unpublished experiments indicate that, even for particle separations of less than a nanometer, the nonlocal theory works well.

Transformation optics has been generalized to deal with these nonlocal effects (*40*). Figure 5 shows the theory applied to a system of two touching silver nanocylinders. Figure 5B shows calculated cross sections for differing degrees of nonlocality, the green curve for δ^{-1} = 0.16 nm being the appropriate value for silver. Evidently in the nonlocal system, the continuous spectrum is replaced by a series of discrete levels. This comes about because surface plasmons are no longer prevented from reaching the touching point, and, when they meet, their phases must match, imposing quantization. The effect grows more evident with increasing nonlocality. In Fig. 5C, we show the enhancement at the touching point as a function of frequency and cylinder radius. As discussed, large cylinders show poor enhancement because of competition from radiative losses. Small cylinders show a pronounced blue shift and reduced enhancement. The optimum choice of radius seems to be in the range 35 nm < R < 80 nm.

Conclusions

Our aim has been to showcase the most recent application of transformation optics, to the design of massively subwavelength systems, with particular examples chosen from plasmonic devices designed to concentrate light. Transformation optics has now found applications to many fields: initially to adaptation of computer programs to varying geometries; then to negative refraction devices and perfect lenses, enormously expanding the potential applications; to the problem of invisibility; and now to subwavelength structures.

The key ingredients of transformation optics are the electric and magnetic field lines. These replace the rays of light that appear in the approximations of Snell's law and ray optics but retain the visual insight while fully satisfying Maxwell's equations. Indeed physical insight is the key benefit of this approach to electromagnetism. Our expectation is that transformation optics will be the design tool of choice in electromagnetic theory.

References and Notes

1. D. M. Shyroki, http://arxiv.org/abs/physics/0307029v1 (2003).
2. D. Schurig, J. B. Pendry, D. R. Smith, *Opt. Express* **14**, 9794 (2006).
3. A. J. Ward, J. B. Pendry, *J. Mod. Opt.* **43**, 773 (1996).
4. J. B. Pendry, *Phys. Rev. Lett.* **85**, 3966 (2000).
5. J. B. Pendry, *Opt. Exp.* **11**, 755 (2003).
6. U. Leonhardt, *Prog. Opt.* **53**, 70 (2009).
7. N. B. Kundtz, D. R. Smith, J. B. Pendry, *Proc. IEEE* **99**, 1622 (2011).
8. U. Leonhardt, *Science* **312**, 1777 (2006); 10.1126/science.1126493.
9. H. Chen, C. T. Chan, *J. Phys. D Appl. Phys.* **43**, 113001 (2010).
10. P. A. Huidobro, M. L. Nesterov, L. Martín-Moreno, F. J. García-Vidal, *Nano Lett.* **10**, 1985 (2010).
11. Y. Liu, T. Zentgraf, G. Bartal, X. Zhang, *Nano Lett.* **10**, 1991 (2010).
12. J. B. Pendry, D. Schurig, D. R. Smith, *Science* **312**, 1780 (2006); 10.1126/science.1125907.
13. M. Fleischmann, P. J. Hendra, A. J. McQuillan, *Chem. Phys. Lett.* **26**, 163 (1974).
14. F. J. García-Vidal, J. B. Pendry, *Phys. Rev. Lett.* **77**, 1163 (1996).
15. J. P. Kottmann, O. J. F. Martin, *Opt. Exp.* **8**, 655 (2001).
16. K. H. Su *et al.*, *Nano Lett.* **3**, 1087 (2003).
17. M. I. Stockman, *Phys. Rev. Lett.* **93**, 137404 (2004).
18. C. E. Talley *et al.*, *Nano Lett.* **5**, 1569 (2005).
19. L. A. Sweatlock, S. A. Maier, H. A. Atwater, J. J. Penninkhof, A. Polman, *Phys. Rev. B* **71**, 235408 (2005).
20. I. Romero, J. Aizpurua, G. W. Bryant, F. J. García de Abajo, *Opt. Exp.* **14**, 9988 (2006).
21. R. T. Hill *et al.*, *Nano Lett.* **10**, 4150 (2010).
22. R. C. McPhedran, D. R. McKenzie, *Appl. Phys. A* **23**, 223 (1980).
23. R. C. McPhedran, W. T. Perrins, *Appl. Phys. A* **24**, 311 (1981).
24. R. C. McPhedran, G. W. Milton, *Proc. R. Soc. London Ser. A* **411**, 313 (1987).
25. E. Prodan, C. Radloff, N. J. Halas, P. Nordlander, *Science* **302**, 419 (2003).
26. J. A. Schuller *et al.*, *Nat. Mater.* **9**, 193 (2010).
27. A. Aubry *et al.*, *Nano Lett.* **10**, 2574 (2010).
28. A. Aubry, D. Y. Lei, S. A. Maier, J. B. Pendry, *Phys. Rev. Lett.* **105**, 233901 (2010).
29. A. Aubry, D. Y. Lei, S. A. Maier, J. B. Pendry, *Phys. Rev. B* **82**, 125430 (2010).
30. D. Y. Lei, A. Aubry, S. A. Maier, J. B. Pendry, *New J. Phys.* **12**, 093030 (2010).
31. V. Ginis, P. Tassin, C. M. Soukoulis, I. Veretennicoff, *Phys. Rev. B* **82**, 113102 (2010).
32. A. I. Fernández-Domínguez, S. A. Maier, J. B. Pendry, *Phys. Rev. Lett.* **105**, 266807 (2010).
33. Y. Luo, D. Y. Lei, S. A. Maier, J. B. Pendry, *Phys. Rev. Lett.* **108**, 023901 (2012).
34. D. Y. Lei, A. Aubry, Y. Luo, S. A. Maier, J. B. Pendry, *ACS Nano* **5**, 597 (2011).
35. Y. Luo, A. Aubry, J. B. Pendry, *Phys. Rev. B* **83**, 155422 (2011).
36. A. Aubry, D. Y. Lei, S. A. Maier, J. B. Pendry, *Phys. Rev. B* **82**, 205109 (2010).
37. I. Romero, J. Aizpurua, G. W. Bryant, F. J. García De Abajo, *Opt. Express* **14**, 9988 (2006).
38. F. Javier García de Abajo, *J. Phys. Chem. C* **112**, 17983 (2008).
39. J. Aizpurua, S. Rivacoba, *Phys. Rev. B* **78**, 035404 (2008).
40. A. I. Fernández-Domínguez, A. Wiener, F. J. García-Vidal, S. A. Maier, J. B. Pendry, *Phys. Rev. Lett.* **108**, 106802 (2012).

Acknowledgments: D.R.S. and J.B.P. were partially supported by the U.S. Army Research Office (grant no. W911NF-09-1-0539); A.A. by the European Community project PHOME (Contract No. 213390); J.B.P. and S.A.M. by the Leverhulme Trust; and S.A.M. by the Engineering and Physical Sciences Research Council.

10.1126/science.1220600